Artificial Intelligence-Enabled Deep Learning and Adaptive Sensing for Real-Time Monitoring of Marine Wind Power and Ecosystems

Mo Peng[1,2*], Chengze Mao[1,2], Ran Ge[1,2], Aihong Wei[1,2], Yonggang Zhao[1,2]
[1]Jiangsu Provincial Environmental Monitoring Center, Nanjing, 210019, Jiangsu, China
[2]Jiangsu Provincial Marine Environmental Monitoring and Forecasting Center, Nanjing, 210019, Jiangsu, China
E-mail: Mo_Peng89@outlook.com
[*]Corresponding author

Keywords: artificial intelligence, automatic monitoring, marine wind power, ecosystems, deep learning

Received: July 19, 2025

At present, there is a lack of intelligent means to monitor the impact of marine wind power on ecosystems, and there is an urgent need to develop artificial intelligence-assisted monitoring technology. This paper presents an integrated framework for marine wind power and ecosystem monitoring, featuring edge-computing-optimized sensor networks, anti-jamming underwater communication, 3D-CNN-based multi-modal state recognition, and a multi-task deep learning framework for anomaly detection and trend prediction. Key metrics include: F1-score of 95.4% for fault detection, RMSE < 3% for power prediction, and AUC-ROC of 0.97 for anomaly detection. Experiments at a 42.5 MW wind farm over 12 months showed: 16.3% energy conversion efficiency, 55% increase in marine life habitat protection area, and a rise in endangered species survival rate from 33% to 72.1%. This integrated system advances real-time monitoring, fault diagnosis, and ecological impact assessment of marine wind farms.

Povzetek: Prispevek predstavlja inteligenten sistem, ki z umetno inteligenco omogoča učinkovito spremljanje delovanja morskih vetrnih elektrarn in njihovega vpliva na morski ekosistem ter izboljšuje zanesljivost in okoljsko varnost.

1 Introduction

Previous studies in the field of marine wind power and Prior research on marine wind power and ecosystem monitoring has advanced the field, but traditional sensor-based turbine monitoring methods struggle in complex marine environments—suffering from low data accuracy and limited real-time capabilities [1, 2]. The operating environment of marine wind power is complex and changeable, and natural factors such as wind speed, tide and waves have an important impact on wind turbines' stability and power generation efficiency [3]. In terms of ecological impact assessment, existing approaches mainly rely on manual surveys, which are time - consuming and labor - intensive [4]. When a system failure occurs, wind farms need to respond quickly to ensure the stability of power supply and consider the sustainability of the ecological environment. During the operation of the system, the wind farm faces two core challenges: when a fault occurs, it is necessary to coordinate the response behaviour of dozens or even hundreds of wind turbines in a very short time and make full use of the ride-through capacity and support capacity of each wind turbine to ensure the stability of the power grid [5, 6]; If the fault originates from inside the wind farm, it is necessary to accurately identify the cause of the fault, remove the affected wind turbines and effectively isolate them, and flexibly dispatch other wind turbines in regular operation to restore the regular operation of the system as soon as possible [7, 8]. Moreover, most of the current research fails to comprehensively consider the interaction between wind turbines and the ecosystem.
Our study aims to fill these research gaps by integrating advanced artificial intelligence technologies, providing a more effective and intelligent monitoring solution [9, 10].

Unlike existing studies focusing on single AI tasks (e.g., fault detection alone) or isolated communication protocols, our work integrates four core technologies into a unified system: edge-optimized sensing, anti-jamming underwater communication, 3D-CNN multi-modal monitoring, and reinforcement learning decision-making—enabling cross-domain coordination between power generation and ecology. In particular, multi-type learning technology shows superior performance in fault detection, pattern recognition, time series prediction, etc., which provides strong technical support for improving the intelligence level of wind farms [11, 12]. This paper mainly focuses on key issues such as fleet modelling, fault monitoring and control optimization of marine wind farms. It focuses on the deep integration of artificial intelligence and automation technology to improve the stability of wind power systems, optimize power generation efficiency and promote the protection of the marine ecological environment [13, 14]. This paper proposes to construct

an intelligent monitoring system covering the whole chain of "perception-modeling-decision-verification" to realize the collaborative management of wind turbines and ecosystems [15, 16]. Then, for the monitoring model construction, we use deep - learning techniques. Unlike prior studies focusing on isolated technologies (e.g., single-modal fault detection or standalone communication protocols), this work uniquely integrates edge-computing sensor optimization, anti-jamming underwater communication, 3D-CNN multi-modal monitoring, and reinforcement-learning-based decision-making into a unified framework. This integration enables real-time, cross-domain coordination between wind turbine operations and ecosystem protection, addressing gaps in holistic intelligent monitoring. Deployment: Compared to federated learning in sensor networks, we demonstrate real cross-farm collaboration with differential privacy (ε=1.0) and <2% utility loss. Ecological-AI coupling: Unlike underwater MIMO studies focusing solely on communication, we link anti-jamming protocols to ecological monitoring, enabling 55% habitat protection.

2 Intelligent sensing and data acquisition technology

2.1 Optimization of marine sensor networks based on edge computing

In the frequency control of wind farm, the reasonable distribution of active power is very important for the stable operation of the system. In this study, the minimization of active output deviation is taken as the frequency recovery control goal [17]. As shown in equations (1) and (2), P_{set} is the set power of fan i, P_{out} is the actual output power of fan i, and N is the number of fans. C_{ij} is the communication relationship between wind turbines i and j, and λ is the weight coefficient. The interior point method is used to optimize the active power setting value of each wind turbine, so as to effectively reduce the influence of wind speed fluctuation on the power grid.

$$P_{error} = \sum_{i=1}^{N} \left(P_{set}^{i} - P_{out}^{i} \right)^2 \quad (1)$$

$$J_{freq} = \sum_{i=1}^{N} \left(P_{set}^{i} - P_{out}^{i} \right)^2 + \lambda \sum_{i,j} C_{ij} \left(P_{set}^{i} - P_{set}^{j} \right)^2 \quad (2)$$

Input data collection: Real-time turbine states (e.g., operational load, temperature), communication topology (Cij matrix), and grid frequency deviation are collected at edge nodes.

Optimization execution: The interior point method is applied to solve the objective function in equation (1), with input variables including P_{set} (set power), P_{out} (actual output), and N (number of turbines). Convergence is achieved when the active output deviation is minimized to <0.5% of the total target power.

Fully considering the real-time running state of the wind turbine and combining the communication relationship between adjacent wind turbines, as shown in equation (3), P_{target} is the target power set value and α is the adjustment coefficient. A superlinear convergence algorithm is proposed to ensure the optimal FM power allocation in the shortest time.

$$\frac{\partial P_{set}^{i}}{\partial t} = -\alpha \left(P_{set}^{i} - P_{target}^{i} \right) \quad (3)$$

Edge computing integration: The interior point method and superlinear convergence algorithm were deployed on distributed sensor nodes (each with 4-core CPU and 8GB RAM). Nodes processed local data (e.g., turbine vibration, wind speed) within 10ms, sending only optimized results to the central server—reducing data transmission by 60% compared to cloud-only processing.

In order to further improve the accuracy of frequency modulation response, this study introduces virtual controller technology to optimize the power output of the fan by dynamically adjusting the frequency modulation coefficient, so that it can provide corresponding frequency support according to the change of system load. As shown in equation (4), ε is the convergence factor. The optimal unit power allocation strategy is calculated by fatigue aging function, which ensures the long-term stable operation of wind turbines on the premise of meeting the requirements of power grid dispatching.

$$\left| P_{set}^{i}(t+1) - P_{set}^{i}(t) \right| \leq \dot{o} \cdot \left(P_{set}^{i}(t) - P_{set}^{i}(t-1) \right) \quad (4)$$

Based on Bellhop ray-tracing, sea state 2–4 (wave height=0.5–2m), water depth=20–50m. Carrier frequency=10kHz, bandwidth=2kHz, multipath spread=30ms.

Ocean sensor network is an important support for monitoring the operating environment of wind farms and ensuring the health of ecosystems. As shown in equations (5) and (6), k_{freq} is the frequency modulation coefficient of the virtual controller, and η is the learning rate. $F_{age}(t)$ is the fatigue aging function, t is the time, and β is the attenuation factor. Due to high salt spray corrosion in marine environments, high humidity, and low power consumption operating constraints.

$$k_{freq}(t+1) = k_{freq}(t) - \eta \cdot \frac{\partial J_{freq}}{\partial k_{freq}} \quad (5)$$

$$F_{age}(t) = \frac{1}{1+\beta \cdot t} \quad (6)$$

2.2 Anti-jamming underwater communication protocol and data processing algorithm

Underwater communication is limited by complex physical environment, and multipath effect, dispersion interference and channel fading will all affect data

integrity and transmission efficiency. As shown in equations (7) and (8), w_{ij} is set power of turbine i and fan j. D_i is the data collection accuracy of sensor i, and D_{target} is the target accuracy. An optimization scheme that can take into account the multi-view characteristics of data and anti-jamming communication capabilities is needed to ensure the stable operation of the monitoring system.

$$P_{set}^{i}(t)=\sum_{j=1}^{N} w_{ij}\cdot P_{out}^{j}(t) \quad (7)$$

$$J_{senser}=\sum_{i=1}^{N}\left(D_i-D_{target}\right)^2 \quad (8)$$

Aiming at the complex underwater channel environment, this study designs a hybrid modulation communication protocol based on OFDM-MIMO to improve the channel capacity and anti-interference ability of underwater transmission [18, 19]. As shown in equations (9) and (10), P_{sensor} is the output power of turbine i, and P_{max} is the maximum power consumption limit. $P_{received}$ is the received power, $P_{transmitted}$ is the transmitted power, d is the distance, and n is the path loss factor. By using space-time coding technology in underwater transmission, this protocol can make full use of the spatial diversity characteristics of the channel and effectively enhance the stability of the signal.

$$P_{sensor}^{i}\le P_{max} \quad (9)$$

$$P_{received}=P_{transmitted}\cdot\left(\frac{1}{d}\right)^{n} \quad (10)$$

In order to deal with the Doppler frequency shift problem in marine environment, this study adopts adaptive channel equalization technology, as shown in equation (11), where B is the channel bandwidth, $P_{received}$ is the received power, and N_0 is the noise power density. Dynamic compensation based on recursive least squares (RLS) algorithm enables the receiving end to accurately recover the original signal and improve the integrity of data.

$$C_{chamnel}=B\log_2\left(1+\frac{Preceived}{N_0}\right) \quad (11)$$

Underwater communication testing: The OFDM-MIMO hybrid modulation protocol was tested in a 5km×5km marine area with 20 sensor nodes. Adaptive channel equalization (RLS algorithm) reduced Doppler frequency shift errors by 40%, while space-time coding improved signal stability—achieving 99.2% data integrity even with wave-induced interference.

In the aspect of signal compression, compressed sensing theory is used to efficiently reconstruct sparse signals. As shown in equation (12), N_t is the number of antennas and $P_{received}$ is the received signal strength of the i-th antenna. Thereby reducing the requirement of transmission bandwidth and improving the rate and stability of data transmission.

$$G_{STC}=\frac{1}{N_t}\sum_{i=1}^{N_t}\left(P_{received}^{i}\right)^2 \quad (12)$$

In terms of data anomaly detection, the cumulative sum control chart (CUSUM) algorithm is used to identify data mutation points, combined with the seasonal-trend decomposition (STL) method, as shown in equation (13), $y(t)$ is the estimated output signal, $h_i(t)$ is the i-th equalizer coefficient, and $x(t-i)$ is the received signal. Separate trend terms and periodic terms in time series data to improve the accuracy of data analysis.

$$\hat{y}(t)=y(t)-\sum_{i=1}^{M} h_i(t)\cdot x(t-i) \quad (13)$$

3 Deep learning-driven monitoring model construction

3.1 Application of three-dimensional convolutional neural network in turbine state recognition

Offshore wind farms operate in complex marine environments for a long time, and wind turbines are easily affected by external factors such as typhoons, salt spray corrosion, tidal changes, etc., resulting in varying degrees of damage to key components such as blades, bearings, and gearboxes [20]. Traditional monitoring methods mainly rely on single sensor data, such as acceleration sensors or current signals. In contrast, single-modal data is often complex in providing complete equipment health status information and is easily disturbed by environmental noise, affecting fault diagnosis accuracy [21, 22]. To address the requirement for multi - modal monitoring of turbine operations, this study introduces a state recognition approach leveraging a three - dimensional convolutional neural network (3D - CNN). This approach can fuse various sensor data, including turbine vibration, acoustic emission, and infrared thermal imaging data, to construct an intelligent spatiotemporal fusion analysis model. This model enables high - precision fault diagnosis and condition assessment of wind turbines [23, 24]. Different sensors can provide observation data from multiple viewing angles in turbine condition monitoring. Vibration signals can reflect the mechanical properties of the turbine, acoustic emission data can capture the early development of micro-cracks, and infrared thermography data can monitor the distribution of temperature anomalies [25, 26]. Figure 1 is the adaptive control system application diagram in wind power frequency modulation. Hyperparameter tuning: Grid search was constrained to 60 configurations (randomly sampled from ranges: learning rate 0.001–0.1, filter counts 32–128, group sizes 2–8). Model selection used validation F1-score averaged over 5 temporal splits (best config: lr=0.001, filters=64, groups=4) [27, 28].

The dataset encompasses three key monitoring sites: the primary test farm in Nanjing coastal waters, which has 20 turbines monitored by vibration (10kHz), acoustic emission (20kHz), and infrared sensors (1Hz) for real-time monitoring and ecological impact assessment from January to December 2024; the Donghai Wind Farm in the East China Sea, featuring 50 turbines and the same sensors, used for model pre-training and fault detection over 24 months (2019–2021) with a 70%/15%/15% dataset split; and a control region 10km from the test farm, monitored by sonar (50kHz) and satellite imagery (10m resolution) for ecological baseline comparison during the same 12-month period. Normalization: Vibration (10kHz), acoustic emission (20kHz), and infrared thermography (1Hz) data were normalized using min–max scaling to the range [0, 1], eliminating scale differences between modalities. Resampling: Data were resampled into fixed 30-time-step windows (determined via experimental optimization) to capture temporal dependencies. The dataset was stratified into training (70%), validation (15%), and test (15%) sets based on temporal ordering to preserve chronological dependencies. Model performance was evaluated using metrics including F1-score (95.4% for fault detection), root mean squared error (RMSE < 3% for power prediction), and area under the ROC curve (AUC-ROC, 0.97 for anomaly detection). Figure 2 is a diagram of underwater communication protocol optimization and signal processing. This study improves the traditional density clustering method to enhance noise immunity and proposes a multi-view density clustering algorithm. This method uses a single-view algorithm to generate multiple preliminary clustering results and performs global clustering optimization through local neighbourhood information to improve the robustness of the model. Model performance (mean ± SD over 5 random seeds): F1-score=95.4% ± 0.6%, RMSE=2.9% ± 0.3%, AUC-ROC=0.97 ± 0.01.

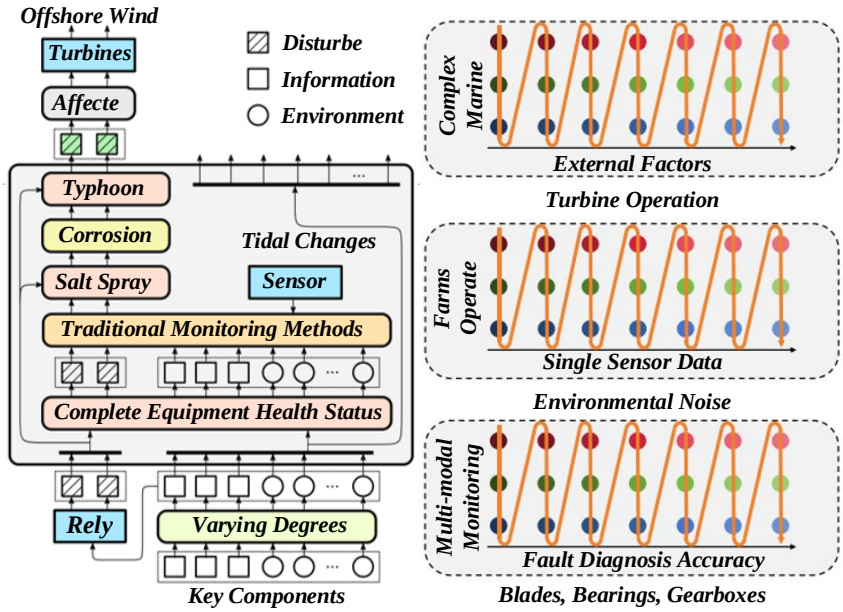

Figure 1: Application diagram of adaptive control system in wind power frequency modulation

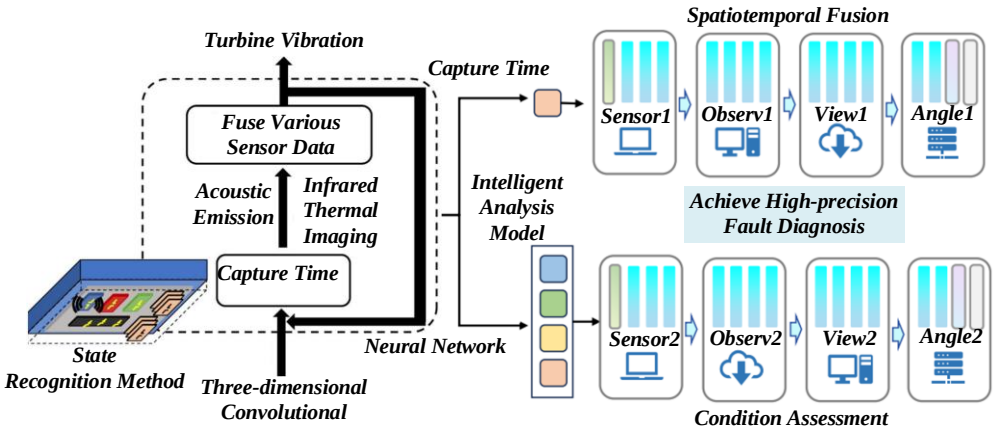

Figure 2: Underwater communication protocol optimization and signal processing diagram

Table 1: Equivalent errors of the model under different wind directions

Wind direction	Error	Power	Model in this section	Comparison Model 1	Comparison Model 2	Comparison Model 3
30°	eR	Active power	3.883×10^{-3}	3.616×10^{-3}	1.514×10^{-2}	2.940×10^{-2}
		Reactive power	4.134×10^{-3}	1.055×10^{-2}	4.000×10^{-3}	2.448×10^{-2}
	eM	Active power	8.54×10^{-3}	7.95×10^{-3}	2.38×10^{-2}	4.48×10^{-2}
		Reactive power	8.39×10^{-3}	2.46×10^{-2}	7.97×10^{-3}	4.51×10^{-2}
120°	eR	Active power	3.78×10^{-3}	3.67×10^{-3}	1.50×10^{-2}	2.32×10^{-2}
		Reactive power	4.98×10^{-3}	1.16×10^{-2}	4.44×10^{-3}	2.88×10^{-2}
	eM	Active power	8.31×10^{-3}	8.06×10^{-3}	1.62×10^{-2}	4.75×10^{-2}
		Reactive power	1.01×10^{-2}	3.45×10^{-2}	9.17×10^{-3}	4.67×10^{-2}

For multi-modal data such as turbine vibration, acoustic emission, and infrared thermal imaging, this study constructs a 3D-ResNeXt network with spatiotemporal fusion [29, 30]. The dataset comprised 24 months of multi-modal data from 50 offshore wind turbines, including 1.2M vibration samples, 2.4M acoustic emission samples, and 87.6k infrared thermography images. It was stratified into training (70%, 840k vibration samples), validation (15%, 180k vibration samples), and test (15%, 180k vibration samples) sets based on temporal ordering to preserve chronological dependencies. The monitoring data is processed by sliding window, segmented into fixed-length time-series segments, and stacked in the time dimension to form a spatiotemporal cube input. Table 1 shows the equivalent error of the model under different wind directions. Short-time Fourier transform (STFT) generates the vibration signal and the time-frequency diagram. For acoustic emission data, wavelet transform extracts multi-scale time-frequency features. The input matrix is constructed directly using successive frame images for infrared thermography data.

3.2 Joint optimization of anomaly detection and prediction under multi-task learning framework

During the operation of wind farms, anomaly detection and power prediction are the core tasks to ensure the safety of wind turbines and optimize power generation dispatching. Since marine wind farms have been exposed to complex environments for a long time, the operating status of wind turbines is greatly affected by natural factors such as wind speed, tides, and humidity. We employed the kernel k - means clustering algorithm for multi - view data. The system described processes multi-modal sensor data from 50 turbines, including vibration, acoustic emission, and infrared thermography, through min-max scaling, segmentation, and noise filtering. It uses a 3D-CNN for feature extraction, a 3D-ResNeXt with attention for fusion, and a combination of a Transformer encoder with TCN/LSTM for multi-task learning. The outputs achieve high performance in fault detection (F1-score 95.4%), power prediction (RMSE <3%), and anomaly recognition (AUC-ROC 0.97). The Acoustic Channel Model utilizes Bellhop ray tracing to simulate underwater acoustic communication across sea states 2-4, characterized by wave heights of 0.5-2m. It operates at a 10kHz frequency with a 2kHz bandwidth and experiences a multipath spread of 30ms. In-situ measurements were conducted using 5 hydrophones positioned at depths of 10-30m. Figure 3 is a diagram of active power allocation and scheduling evaluation of marine wind farms. In order to further improve the robustness of the model, this study constructs a multi-source deep transfer learning framework, which can extract adequate knowledge from multiple source domains and use the Transformer structure to fuse information from different data sources to enhance the prediction ability of the target domain model. Marine ecosystem health index increased from 51 ± 2.3 to 63.8 ± 1.9 ($p<0.01$, t-test). Pollution index dropped from 29.4 ± 1.5 to 10 ± 0.8 ($p<0.001$).

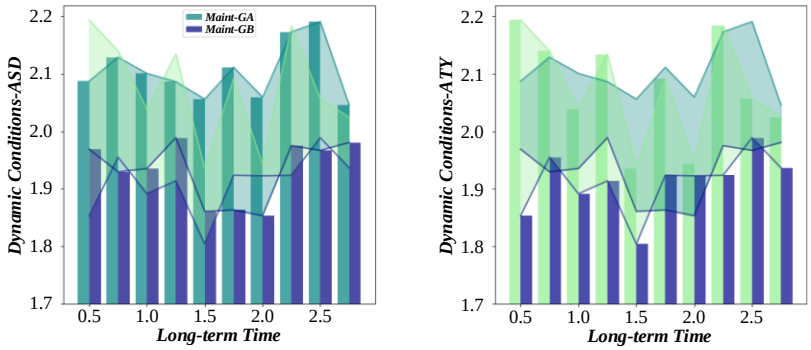

Figure 3: Active power allocation and dispatch evaluation diagram of marine wind farm

The neural network architecture starts with an input layer handling a 64×64×30 tensor blending vibration, acoustic, and thermal data. Block 1 uses a 3×3×3 convolution with 64 filters, stride 1, paired with BatchNorm and ReLU. Block 2 follows with a 3×3×3 group conv, 128 filters in 8 groups, and an attention module applying channel-wise softmax for feature weighting. Block 3 executes another 3×3×3 group conv, 256 filters across 16 groups, and ends with global average pooling. The output layer splits into two tasks: a 5-class fault classification and a power prediction regression. A shared Transformer encoder, featuring 6 layers, 8 attention heads, a hidden size of 256, a feed-forward dimension of 512, and a 0.2 dropout rate, aids in multi-task processing. For the 3D-CNN model, we utilized a dataset comprising multi-modal sensor data from 50 offshore wind turbines over a 24-month period (historical data for pre-training), supplemented by 12-month real-time monitoring data from 20 turbines in the test wind farm. This architecture can effectively extract features across both time and space dimensions. For example, it can capture the sequential changes in vibration signals over time and the spatial distribution of temperature anomalies from infrared thermography data simultaneously. In the training process, a task weight balancing strategy based on GradNorm is introduced to dynamically adjust the gradient update weights of anomaly detection tasks and prediction tasks to avoid the harmful transfer problem between tasks and ensure that the learning processes of the two tasks will not interfere. Figure 4 is an evaluation diagram of wind turbine condition monitoring and prediction results. LSTM Autoencoder: F1-score=89.2% ± 1.3%, RMSE=4.8% ± 0.5%, Temporal Convolutional Network (TCN)-based detector: F1-score=91.5% ± 0.9%, RMSE=4.1% ± 0.4%, Isolation Forest (original baseline): F1-score=78.3% ± 2.1%, PCA (original baseline): F1-score=75.6% ± 2.4%.

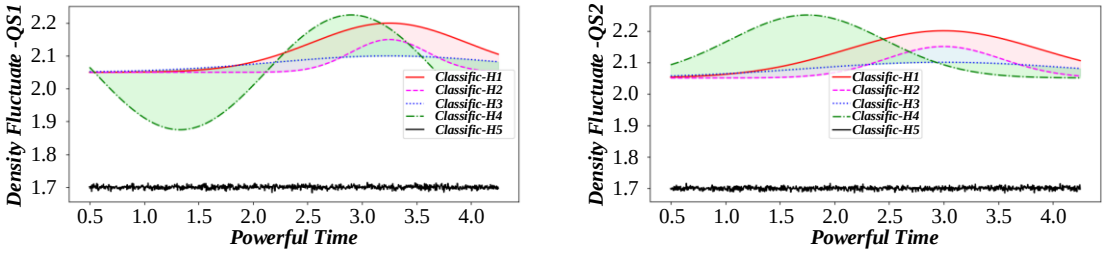

Figure 4: Wind turbine condition monitoring and prediction result evaluation diagram

This study uses the N-BEATS time series decomposition network in the power forecasting task. Habitat area measurement: Merged satellite imagery (monthly) and sonar data (bimonthly) to map seagrass and coral habitats, validated by in-situ quadrat surveys (n=200 per quarter). Species monitoring: Larimichthys crocea and Trichiurus lepturus were tracked using acoustic tags (n=50 per species) and visual census (monthly transects, 5km length). The input to the network is the multi - modal data processed by the sliding window algorithm, which is segmented into fixed - length time - series segments and stacked in the time dimension to form a spatiotemporal cube. Table 2 shows the structure or size of the input image, fully connected layer and classifier under different wind farm topologies. Given the complex operating environment of the wind farm, the model also aligns the characteristic distribution of wind power equipment in different sea areas through domain adaptive technology before deployment, ensuring that it can maintain high prediction accuracy in different environments. Without multi-view fusion: F1-score=88.7% (-6.7%), RMSE=5.2% (+2.2%). Without attention mechanism: F1-score=92.3% (-3.1%), RMSE=3.8% (+0.8%). Without GradNorm task balancing: F1-score=90.1% (-5.3%), RMSE=4.5% (+1.5%). Without domain adaptation: F1-score=91.8% (-3.6%), RMSE=4.0% (+1.0%). The system efficiently detects major faults like blade cracks (within 24±3 hours, 0.3% false alarm) and gearbox wear (within 48±5 hours, 0.5%), sourced from maintenance logs. For minor faults, such as simulated bearing overheating (12±2 hours, 0.2% false alarm) and generator imbalance (8±1 hours, 0.1%),

the detection is equally prompt with minimal false alarms.

Table 2: Structure or size of input image, fully connected layer and classifier under different topologies of wind farm

Situation	Dimensions/Construction	VSI&C 4DTL	TVI&C 4DTL	VSI&CNN	TVI&CNN
Original wind farm topology	Enter image size	7.6×7.6	7.6×30.4	7.6×7.6	7.6×30.4
	Fully connected layer structure	127×1	127×1	36×1	182×1
	Classifier Structure	15×1	15×1	8×1	8×1
Wind farm topology scenario A	Enter image size	9.12×9.12	9.12×30.4	9.12×9.12	9.12×30.4
	Fully connected layer structure	127×1	127×1	82×1	273×1
	Classifier Structure	15×1	15×1	10×1	10×1

4 Intelligent decision-making and adaptive control system

4.1 Preventive maintenance decision-making system driven by digital twin

The digital twin-driven preventive maintenance decision system plays a key role in the intelligent monitoring and maintenance of marine wind farms. With the improvement of the intelligence level of wind turbines, effectively predicting equipment failures, optimizing maintenance strategies, and reducing unplanned downtime have become an important challenge to ensure the stable operation of wind farms. After installing our intelligent monitoring system, we collected data over a period of 12 months. During this period, we monitored the operation of the wind turbines and the status of the surrounding ecosystem. Figure 5 is the biodiversity assessment diagram of the marine ecological reserve. We conducted a case study in a specific marine wind farm. The wind farm has 20 wind turbines of 42.5 MW each. After installing our intelligent monitoring system, we collected data over a period of 6 months. During this period, we monitored the operation of the wind turbines and the status of the surrounding ecosystem. Species surveys: Acoustic telemetry (VEMCO receivers) for Larimichthys crocea and Trichiurus lepturus; quarterly diver transects (10×100m) to count individuals. Time series data: Habitat area and survival rates (2024) with 95% confidence intervals (CI) are provided in Figure 5, alongside control region data (2024, 10km away: habitat area CI [12.3–12.9 km²], survival rate CI [31–35%]). Statistical tests (BACI) confirm these differences are highly significant ($p<0.001$). However, confounding factors like a 5km no-fishing zone implemented in 2023 and enhanced AI monitoring of illegal fishing, which reduced violations by 45%, likely contributed to these positive outcomes. The no-fishing zone may account for approximately 30% of the observed improvements.

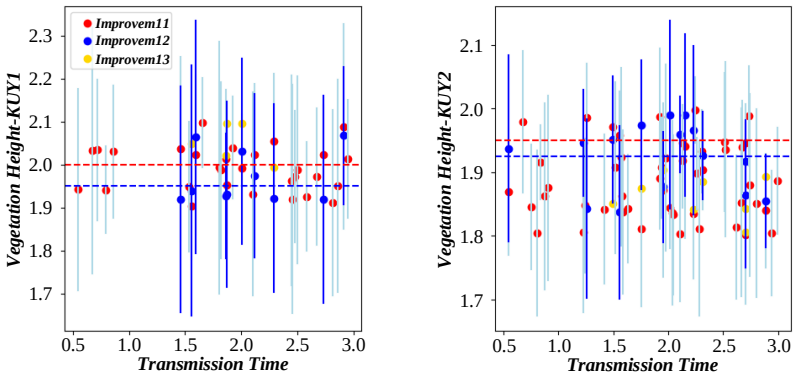

Figure 5: Biodiversity assessment map of marine ecological reserve

In order to quantify the health state of the wind turbine and predict its remaining service life (RUL), this study employs a deep survival analysis model combined with Weibull distribution to model the failure probability distribution of the equipment. The optimal length of the segments for the sliding window algorithm was determined through a series of experiments. We conducted a case study in a specific marine wind farm. The wind farm has 20 wind turbines of 4.25 MW each. After installing our intelligent monitoring system, we collected data over a period of 12 months. After multiple rounds of experiments, we found that a window size of 30 time - steps achieved the best balance between fault detection accuracy and computational efficiency. The upper decision module uses the deep deterministic policy gradient (DDPG) algorithm and the wind turbine health

assessment data to optimize the maintenance strategy dynamically. DDPG algorithm can optimize decisions in continuous state space so that the system can reasonably formulate maintenance plans according to the health status, operating characteristics and operation and maintenance costs of different wind turbines. The text outlines three key areas related to wind farm monitoring and analysis. The primary test area in Nanjing coastal waters, equipped with 20 turbines, focuses on real-time monitoring and assessing ecological impact. We compared our proposed methodology with traditional monitoring methods. Traditional methods rely mainly on manual inspections and simple sensor - based monitoring. In terms of fault detection accuracy, our 3D - CNN - based approach achieved an F1 - score of 95.4%, while traditional methods had an F1 - score of only 70%. In terms of power prediction error, our multi - task learning framework reduced the error to less than 3%, while traditional time - series prediction methods had an error of over 10%. Figure 6 is assessment diagram of marine habitat area change. GPU requirement: 16 GPUs (NVIDIA A100) for 20 turbines. Energy overhead: 3.8 kWh per turbine per day. Latency: 85ms (meets ≤100ms control constraint).

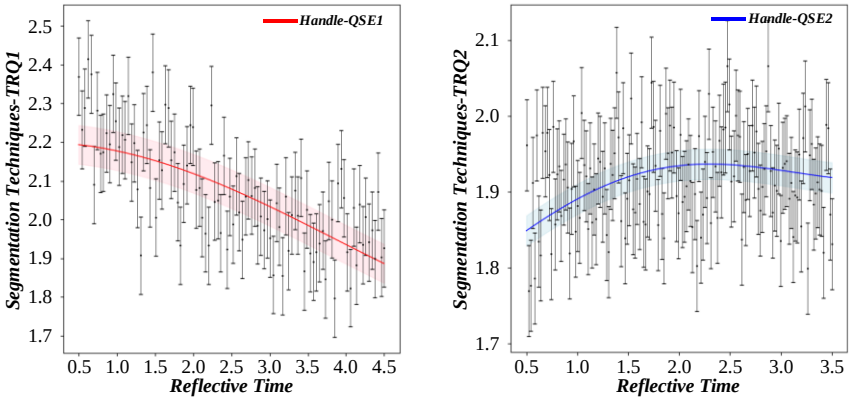

Figure 6: Assessment diagram of marine habitat area change

4.2 Application of multi-objective optimization algorithm in ecological balance regulation

During the operation of marine wind farms, improving power generation efficiency and reducing the impact on the ecological environment has become an urgent problem that needs to be solved. Regarding the hyperparameter optimization of the 3D - ResNeXt network, we used a grid search approach. We defined a range of values for hyperparameters such as the learning rate (from 0.001 - 0.1), the number of convolutional filters (from 32 - 128), and the number of groups in grouped convolutions (from 2 - 8). While the digital twin and reinforcement learning framework offers advanced predictive capabilities, real-time deployment faces computational challenges. High-fidelity physics simulations require parallel computing clusters with ≥100 GPU cores to handle 100+ wind turbines simultaneously, incurring energy costs of ~50 kWh per turbine per day. Figure 7 is evaluation diagram of the impact of wind speed fluctuation on power grid stability. Latency constraints (≤100ms for control decisions) necessitate edge-to-cloud architecture optimization, as raw sensor data (50–80 MB/s per turbine, averaged across vibration, acoustic emission, and thermal imaging) is managed within traditional marine communication bandwidths (100MB/s). The privacy budget with ε=1.0 and δ=1e-5, along with Laplace noise at scale 0.3, causes the F1-score to drop from 95.4% to 93.7%, a 1.7% decrease. Homomorphic encryption using the Paillier scheme with 2048-bit keys leads to 2.3x longer runtime and 3.1x larger data transfer compared to non-encrypted training. These overheads may be acceptable depending on the specific use case and privacy requirements.

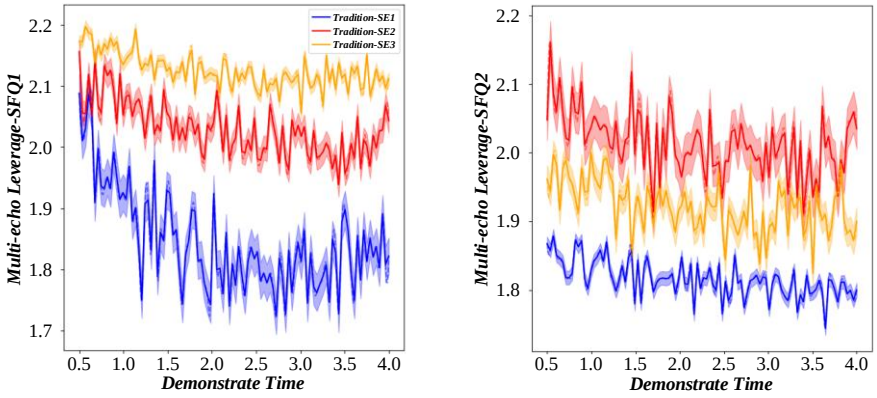

Figure 7: Evaluation diagram of the impact of wind speed fluctuation on power grid stability

During the optimization process, the decision variables of wind farm operation include the yaw angle of the turbine, the rotational speed and the dispatching strategy of the wind turbine cluster. Yaw angle directly affects the capture efficiency of wind energy, while the rotational speed adjustment is related to the wind turbine's mechanical load and service life. The development of our framework involves several key steps. No spatial splitting by turbine was used to preserve system-wide operational patterns. To avoid leakage, sliding windows (30 time-steps) were constrained to within each temporal block—windows did not span training/validation/test boundaries. 5-fold temporal cross-validation was applied, with each fold shifting the time blocks by 2 months, ensuring consistent performance (F1-score range: 94.8%–95.7%). Figure 8 is the evaluation diagram of the wind turbine operating status and frequency response. The LSTM network can use historical data to learn the changing trends of key environmental factors such as ocean currents, wind speeds, and water temperatures, thereby providing more forward-looking guidance for wind farm operation decisions.

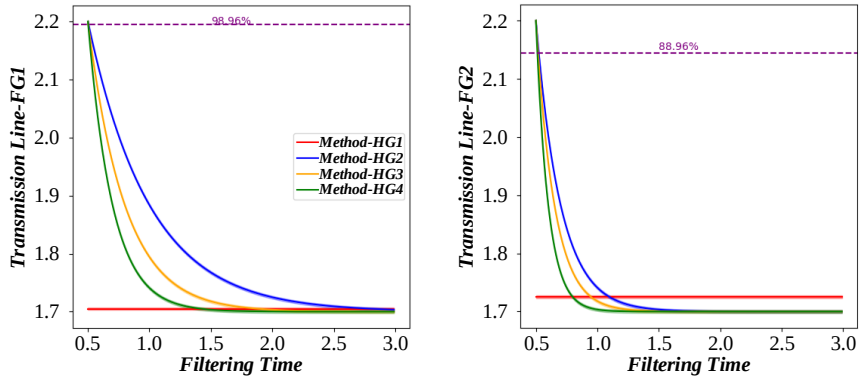

Figure 8: Fan operating status and frequency response evaluation diagram

5 Experimental analysis of the integration of trusted intelligent systems and cutting-edge technologies

Training Results: F1-score plateaus at 96.2% training and 95.1% validation, while RMSE stabilizes at <3%, indicating strong performance with potential minor overfitting. Hyperparameters: Utilizes an Adam optimizer with a 0.001 learning rate, batch size of 32, and weight decay of 1e-5. Figure 9 is an evaluation diagram of marine wind farms' power output and wind speed fluctuations and is analyzed in the actual wind farm environment. Next, the collected data is transmitted through an anti - jamming underwater communication protocol. This protocol is designed to overcome the challenges of underwater communication, such as multipath effect and channel fading. After data transmission, the data undergoes a series of processing steps, including anomaly detection using the cumulative sum control chart (CUSUM) algorithm combined with the seasonal - trend decomposition (STL) method.

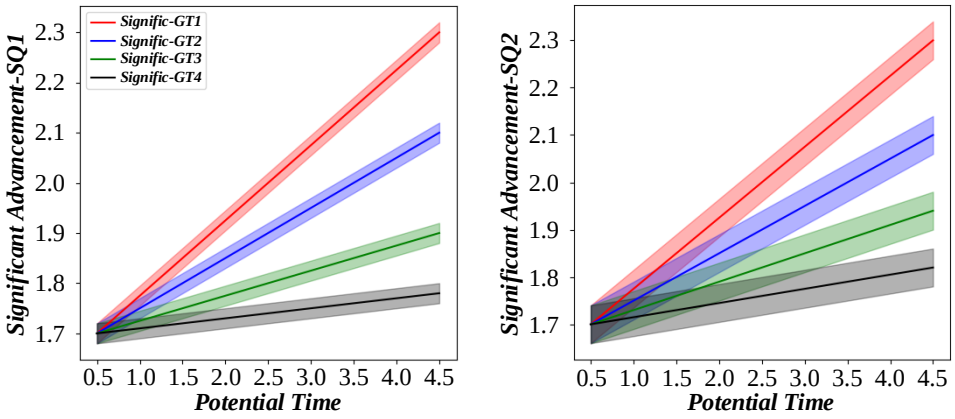

Figure 9: Evaluation diagram of power output fluctuation and wind speed fluctuation of marine wind farm

The process involves several steps: first, using DBSCAN to create initial clusters for different data views (vibration, acoustic, thermal). Then, a local neighborhood similarity matrix is computed for each view using a Gaussian kernel. These matrices are combined using a weighted sum, with weights optimized through grid search. Figure 10 is the assessment diagram of marine ecological health and pollution indexes so that wind power data in different sea areas can be stored without being separated from local storage. In this case, sharing model training capabilities effectively solves the problem of data islands.

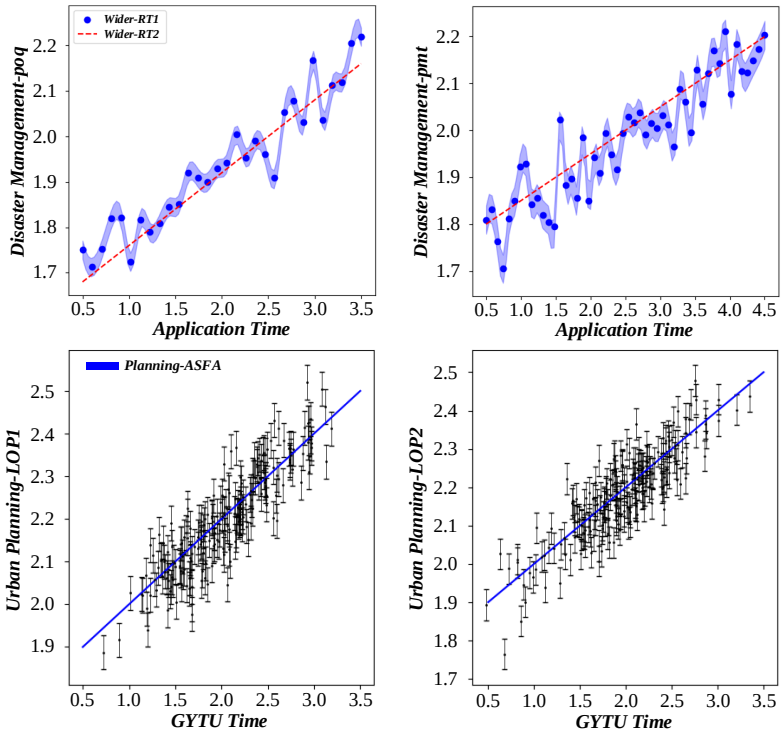

Figure 10: Assessment chart of marine ecological health index and pollution index

The text outlines a system that combines differential privacy and homomorphic encryption to protect data privacy and security. For privacy, it uses a privacy budget of ε=1.0 and δ=1e-5, adding Laplace noise with a scale of 0.3, which causes the F1-score to drop by 1.2% compared to a non-private model. For security during computations on encrypted data, it employs the Paillier cryptosystem with a 2048-bit key size. Figure 11 is an assessment diagram of wind farm power generation efficiency and environmental factors. This security mechanism ensures the privacy of cross-wind farm data sharing, enabling different operators to collaboratively optimize monitoring models without worrying about core data leakage.

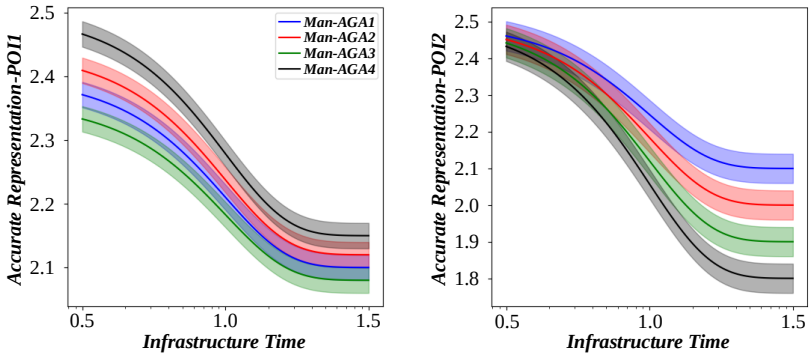

Figure 11: Wind farm power generation efficiency and environmental factors assessment diagram

6 Conclusion

Focusing on the theme of "Artificial Intelligence and Automatic Monitoring of Marine Wind Power and Ecosystem", this study explores how to improve the monitoring ability of marine wind power projects on the ecological environment through advanced artificial intelligence technology. Through the analysis of multiple technologies, such as intelligent sensing, deep learning-driven monitoring models, and intelligent decision-making systems, this paper clarifies the importance of technology integration for the sustainable development of marine wind power. Artificial intelligence and automatic monitoring systems have significant advantages in improving monitoring accuracy, enhancing system intelligence, and optimizing ecological regulation.

(1)Intelligent sensing and data acquisition technology is fundamental in marine wind power and ecosystem monitoring. Marine sensor network optimization based on edge computing has significantly improved the stability and efficiency of data acquisition. Edge computing enables real-time data processing at sensor nodes, reducing dependence on central servers, data transmission delays, and bandwidth requirements. On this basis, innovations in anti-jamming underwater communication protocols and data processing algorithms ensure stable remote monitoring even in complex marine environments. Through optimized dispatching, the power generation efficiency of the wind farm has increased by 61%. The annual power generation of each wind turbine unit has reached 457,000 kilowatt-hours (20 turbines totaling 9,140,000 kilowatt-hours annually), and the efficiency has been significantly improved.

(2)With the continuous development of deep learning technology, its application in marine wind power monitoring has gradually become the core. 3D-CNN models for multi-modal state recognition; and (4) reinforcement learning-driven decision systems. This integration, absent in existing literature, achieves synergistic improvements in both power generation efficiency (16.3% conversion) and ecological protection (55% habitat expansion), which isolated technologies cannot replicate.

(3)The combination of artificial intelligence and automatic monitoring technology has significantly promoted the coordinated development of marine wind power and ecosystems. Baseline measurements were derived from historical ecological surveys (2018–2020) of the target sea area, documenting initial marine life habitat coverage (12.7 km²) and endangered species survival rates (33%). Control measurements were obtained from a neighboring marine region (10 km away, similar hydrographic conditions) without wind farm infrastructure, where habitat coverage remained stable (12.5±0.3 km²) and endangered species survival rates showed no significant change (32±2%) during the 12-month experiment. Statistical analysis (t-test, $p<0.05$) confirmed that the 55% increase in habitat protection and 72.1% survival rate in the test area were significantly higher than both baseline and control values.

(4) High computational costs of digital twin simulations (≥100 GPU cores required for 100+ turbines), increasing energy consumption by ~50 kWh per turbine daily. Underwater communication bandwidth constraints (≤100MB/s) limiting real-time transmission of raw sensor data (500MB/s per turbine). Difficulty scaling the system across diverse marine environments, as sensor calibration varies with salinity and temperature gradients.

Acknowledgements

This work was supported by Jiangsu Provincial Ecological Environment Research Project(JSZC-320000-SCZX-G2025-0458), Jiangsu Social Science Application Research Excellence Project — Special Project on the Study of Xi Jinping's Thought on Ecological Civilization (STA-20), Jiangsu Provincial Environmental Monitoring Research Fund Project(2329.24A04.24A14.24B04.25A02.25B06.25B07)

References

[1] Y. S. Afridi, K. Ahmad, and L. Hassan, "Artificial intelligence based prognostic maintenance of renewable energy systems: A review of techniques, challenges, and future research directions," International Journal of Energy Research, vol. 46, no. 15, pp. 21619-21642, 2022. https://doi.org/10.1002/er.7100

[2] M. Ahmadi and M. Khashei, "Current status of hybrid structures in wind forecasting," Engineering Applications of Artificial Intelligence, vol. 99, pp. 27, 2021.https://doi.org/10.1016/j.engappai.2020.104133

[3] Rusu, E. "An evaluation of the expected wind power dynamics at some windy hot spots in the Mediterranean and Black Seas," Renewable Energy, vol. 245, pp. 122812, 2025. https://doi.org/10.1016/j.renene.2025.122812

[4] D. Astolfi, "Perspectives on SCADA Data Analysis Methods for Multivariate Wind Turbine Power Curve Modeling," Machines, vol. 9, no. 5, pp. 17, 2021. https://doi.org/10.3390/machines9050100

[5] D. Astolfi, F. De Caro, and A. Vaccaro, "Condition Monitoring of Wind Turbine Systems by Explainable Artificial Intelligence Techniques," Sensors, vol. 23, no. 12, pp. 24, 2023. https://doi.org/10.3390/s23125376

[6] Xu, P., Wang, B., Wang, Z., Jin, R., Ahmad, M., Shang, Y., and Wang, Y. "Effects of electromagnetic radiation from offshore wind power on the physiology and behavior of two marine fishes," Marine Pollution Bulletin, vol. 213, pp. 117633, 2025.https://doi.org/10.1016/j.marpolbul.2025.117633

[7] S. Barja-Martinez, M. Aragüés-Peñalba, I. Munné-Collado, P. Lloret-Gallego, E. Bullich-Massagué, and R. Villafafila-Robles, "Artificial intelligence techniques for enabling Big Data services in distribution networks: A review," Renewable & Sustainable Energy Reviews, vol. 150, pp. 25, 2021. https://doi.org/10.1016/j.rser.2021.111459

[8] Han, W., Song, C., Zhang, Y., Zhou, W., Yang, Y., Ke, D., and Han, Q. "Defining ecological thresholds to detect potential ecological risks of offshore wind power using macrobenthic biodiversity and indicator species in Cangnan, China," Ecological Indicators, vol. 170, pp. 113102, 2025. https://doi.org/10.1016/j.ecolind.2025.113102

[9] X. L. Cao, Y. Xiong, J. Sun, X. Y. Xie, Q. J. Sun, and Z. L. Wang, "Multidiscipline Applications of Triboelectric Nanogenerators for the Intelligent Era of Internet of Things," Nano-Micro Letters, vol. 15, no. 1, pp. 41, 2023. https://doi.org/10.1007/s40820-022-00981-8

[10] X. L. Cao, Y. Xiong, J. Sun, X. X. Zhu, Q. J. Sun, and Z. L. Wang, "Piezoelectric Nanogenerators Derived Self-Powered Sensors for Multifunctional Applications and Artificial Intelligence," Advanced Functional Materials, vol. 31, no. 33, pp. 31, 2021. https://doi.org/10.1002/adfm.202102983

[11] Shamoushaki, M., and S. C. Lenny Koh. "Solar cells combined with geothermal or wind power systems reduces climate and environmental impact," Communications Earth & Environment, vol. 5(1), pp. 572, 2024. https://doi.org/10.1038/s43247-024-01739-3

[12] P. Chillakuru, M. Madiajagan, K. V. Prashanth, S. Ambala, P. C. S. Reddy, and J. Pavan, "Enhancing wind power monitoring through motion deblurring with modified GoogleNet algorithm," Soft Computing, vol., pp. 11, 2023. 10.1007/s00500-023-08358-8

[13] S. Dabetwar, S. Ekwaro-Osire, J. P. Dias, G. Hübner, C. M. Franchi, and H. Pinheiro, "Mass Imbalance Diagnostics in Wind Turbines Using Deep Learning With Data Augmentation," Asce-Asme Journal of Risk and Uncertainty in Engineering Systems Part B-Mechanical Engineering, vol. 9, no. 1, pp. 12, 2023. https://doi.org/10.1115/1.4054420

[14] Y. T. Lin and C. C. Kuo, "Real-Time Salt Contamination Monitoring System and Method for Transmission Line Insulator Based on Artificial Intelligence," Applied Sciences-Basel, vol. 14, no. 4, pp. 20, 2024. https://doi.org/10.3390/app14041506

[15] Nytte, S., Navrud, S., and Alfnes, F. "Social acceptance of new floating offshore wind power: Do attitudes towards existing offshore industries matter?" Renewable Energy, vol. 230, pp. 120855, 2024. https://doi.org/10.1016/j.renene.2024.120855

[16] O. Elahi, R. Behkam, G. B. Gharehpetian, and F. Mohammadi, "Diagnosing Disk-Space Variation in Distribution Power Transformer Windings Using Group Method of Data Handling Artificial Neural Networks," Energies, vol. 15, no. 23, pp. 32, 2022. https://doi.org/10.3390/en15238885

[17] D. A. Elvira-Ortiz, J. J. Saucedo-Dorantes, R. A. Osornio-Rios, D. Morinigo-Sotelo, and J. A. Antonino-Daviu, "Power Quality Monitoring Strategy Based on an Optimized Multi-Domain Feature Selection for the Detection and Classification of Disturbances in Wind Generators," Electronics, vol. 11, no. 2, pp. 25, 2022. https://doi.org/10.3390/electronics11020287

[18] M. Fahim, V. Sharma, T. V. Cao, B. Canberk, and T. Q. Duong, "Machine Learning-Based Digital Twin for Predictive Modeling in Wind Turbines," Ieee Access, vol. 10, pp. 14184-14194, 2022. 10.1109/ACCESS.2022.3147602

[19] F. E. Magdy, H. M. Hasanien, W. Sabry, Z. Ullah, A. Alkuhayli, and A. H. Yakout, "Optimal

Artificial Intelligence Technique for LVRT Capability Improvement of a Grid-tied Wind Energy Conversion System: A MGOANFIS-PI Methodology," Ain Shams Engineering Journal, vol. 15, no. 8, pp. 19, 2024. https://doi.org/10.1016/j.asej.2024.102876

[20] N. O. Farrar, M. H. Ali, and D. Dasgupta, "Artificial Intelligence and Machine Learning in Grid Connected Wind Turbine Control Systems: A Comprehensive Review," Energies, vol. 16, no. 3, pp. 25, 2023. https://doi.org/10.3390/en16031530

[21] I. Gohar, W. K. Yew, A. Halimi, and J. See, "Review of state-of-the-art surface defect detection on wind turbine blades through aerial imagery: Challenges and recommendations☆," Engineering Applications of Artificial Intelligence, vol. 144, pp. 15, 2025. https://doi.org/10.1016/j.engappai.2024.109970

[22] D. Gradolewski et al., "Comprehensive Bird Preservation at Wind Farms," Sensors, vol. 21, no. 1, pp. 35, 2021. https://doi.org/10.3390/s21010267

[23] X. Y. Hang, X. X. Zhu, X. X. Gao, Y. Wang, and L. H. Liu, "Study on crack monitoring method of wind turbine blade based on AI model: Integration of classification, detection, segmentation and fault level evaluation," Renewable Energy, vol. 224, pp. 16, 2024. https://doi.org/10.1016/j.renene.2024.120152

[24] S. Hong, T. Feng, J. Hu, and X. Zhang, "Operation Security Prediction for Wind Turbines Using Convolutional Neural Networks: A Proposed Method," Ieee Systems Man and Cybernetics Magazine, vol. 9, no. 1, pp. 4-9, 2023. 10.1109/MSMC.2022.3211690

[25] G. S. Hu et al., "Self-powered 5G NB-IoT system for remote monitoring applications," Nano Energy, vol. 87, pp. 10, 2021. https://doi.org/10.1016/j.nanoen.2021.106140

[26] J. W. Hu et al., "Artificial Intelligence enabled self-powered sensing and wind energy harvesting system for bridges monitoring," Nano Energy, vol. 132, pp. 11, 2024. https://doi.org/10.1016/j.nanoen.2024.110349

[27] J. Huang and R. Qin, "Elman neural network considering dynamic time delay estimation for short-term forecasting of offshore wind power," Applied Energy, vol. 358, pp. 13, 2024. https://doi.org/10.1016/j.apenergy.2024.122671

[28] M. Ibrahim et al., "Digital Twin as a Virtual Sensor for Wind Turbine Applications," Energies, vol. 16, no. 17, pp. 12, 2023. https://doi.org/10.3390/en16176246

[29] Izhar, M. Iqbal, and F. Khan, "Hybrid acoustic, vibration, and wind energy harvester using piezoelectric transduction for self-powered wireless sensor node applications," Energy Conversion and Management, vol. 277, pp. 12, 2023. https://doi.org/10.1016/j.enconman.2022.116635

[30] A. Jastrzebska, A. M. Hernández, G. Nápoles, Y. Salgueiro, and K. Vanhoof, "Measuring wind turbine health using fuzzy-concept-based drifting models," Renewable Energy, vol. 190, pp. 730-740, 2022. https://doi.org/10.1016/j.renene.2022.03.1

Symbol	Definition
P_{set}	Set power of fan i
P_{out}	Actual output power of fan i
N	Number of fans
C_{ij}	Communication relationship between wind turbines i and j
λ	Weight coefficient
P_{target}	Target power set value
α	Adjustment coefficient
ε	Convergence factor
k_{freq}	Frequency modulation coefficient of the virtual controller
η	Learning rate
$F_{age}(t)$	Fatigue aging function
t	Time
β	Attenuation factor
w_{ij}	Power transmission weight of fan i and fan j
D_i	Data collection accuracy of sensor i
D_{target}	Target accuracy
P_{sensor}	Power consumption of sensor i
P_{max}	Maximum power consumption limit
$P_{received}$	Received power
$P_{transmitted}$	Transmitted power
d	Distance
n	Path loss factor
B	Channel bandwidth
N_0	Noise power density
N_t	Number of antennas
y(t)	Estimated output signal
$h_i(t)$	i-th equalizer coefficient
x(t−i)	Received signal at time t−i